Bio-Tribo-Acoustic Emissions: Condition Monitoring of a Simulated Joint Articulation

Olorunlambe, K.a.; Eckold, D.g.; Shepherd, D.e.t.; Dearn, K.d.

DOI:
10.1016/j.biotri.2022.100217

Document Version
Publisher's PDF, also known as Version of record

Citation for published version (Harvard):
Olorunlambe, KA, Eckold, DG, Shepherd, DET & Dearn, KD 2022, 'Bio-Tribo-Acoustic Emissions: Condition Monitoring of a Simulated Joint Articulation', *Biotribology*, vol. 32, 100217.
https://doi.org/10.1016/j.biotri.2022.100217

Biotribology 32 (2022) 100217

Contents lists available at ScienceDirect

Biotribology

journal homepage: www.elsevier.com/locate/biotri

Bio-Tribo-Acoustic Emissions: Condition Monitoring of a Simulated Joint Articulation

K.A. Olorunlambe [a,b], D.G. Eckold [a], D.E.T. Shepherd [b], K.D. Dearn [a,*]

[a] Mechanical Innovation and Tribology Group, Department of Mechanical Engineering, School of Engineering, University of Birmingham, Birmingham, UK
[b] Biomedical Engineering Group, Department of Mechanical Engineering, School of Engineering, University of Birmingham, Birmingham, UK

ARTICLE INFO

Keywords:
Acoustic emission
Artificial joints
Biotribology
NARX neural network
K-means clustering

ABSTRACT

Acoustic emissions have been used to interpret the frictional processes observed in a simulated metal-on-polymer joint replacement articulation during *in vitro* testing. The coefficient of friction profile is predicted from AE features using a nonlinear autoregressive neural network with an external input model, and the evolution of surface damage is identified using k-means clustering of the distribution of emission types from running-in to prolonged sliding states. The predicted coefficient of friction profiles were found to exhibit a similar response to the actual coefficient of friction profiles. Clustering showed that a higher percentage of continuous emissions are generated during the prolonged sliding stage, indicating sliding friction being the most dominant process during that state. The findings of this study provide a significant pathway toward achieving the potential of AE testing as a more intuitive and dynamic process of monitoring the tribological conditions of artificial joints and diagnosing the pathologies of the natural joints.

1. Introduction

Total disc replacement surgeries are usually carried out when joint pathologies such as degenerative disc disease become too severe to be treated using conventional methods. Tribological interactions are fundamental to the operation of these artificial joints, and wear is a principal means of failure, as shown in Table 1. The condition of artificial joints is traditionally evaluated using CT (computed tomography) scans, X-rays and, in some cases, nuclear scanning tests. These diagnostic methods are expensive, time-consuming, and harmful to health due to frequent radiation exposure [15,16,30,31,33,34]. Another concern with these traditional diagnostic methods is that signs of failure do not present early enough to prevent pathologies, causing patients to experience pain and leading to other medical complications due to the migration of wear debris into the bloodstream [1,10,27]. Wear debris from a polymer on metal joint replacements has also been shown to cause aseptic loosening in artificial joints [17]. Thus, there is a need for a simplified, dynamic, and faster way of non-invasively monitoring the condition of artificial joints to avoid these problems; acoustic emission (AE) testing can fulfil this need.

Acoustic emission (AE) testing is a non-destructive test (NDT) method used in the detection of the onset and progression of mechanical flaws [21,41]. It involves using piezoelectric sensors to capture the high-frequency acoustic waves produced by materials undergoing damage due to mechanical loading. These acquired waves are passed through a pre-amplifier for amplification, followed by signal conditioning and event detection (Fig. 1). Some of the wear mechanisms AE has been used to detect include [41]:

- in transmission systems - scuffing, pitting fatigue and bearing wear;
- in machine tool monitoring - flank, abrasive and crater wear.

AE has proven advantageous for analysing and understanding tribological interactions in mechanical systems. It has been used to distinguish between adhesive and abrasive wear modes in polymer-metal pairs, to distinguish between running-in, steady-state and rapid wear stages in metal-metal pairs, and to investigate the influence of various polymeric gear materials on the sound frequency spectrum [6,22,24]. Studies have also shown that a correlation can be found between AE and wear rate, suggesting the possibility of being able to infer mass loss from AE parameters such as signal energy [7,8,20].

In orthopaedic applications, the AE test method has been used to study the tribology of human joints and monitor artificial joints' conditions. AE has been used to predict bone fracture [2,48] and to study

* Corresponding author.
E-mail address: k.d.dearn@bham.ac.uk (K.D. Dearn).

https://doi.org/10.1016/j.biotri.2022.100217
Received 14 February 2022; Received in revised form 30 June 2022; Accepted 3 July 2022
Available online 6 July 2022

Table 1
Total disc replacement failure mode, and their corresponding causes. Collated from [45].

Failure Mode	Cause of Failure
Degradation	Wear and corrosion
Inflammation	Presence of large UHMWPE wear particles
Surface wear and damage	Adhesive and abrasive wear
Damaged UHMWPE core	Plastic deformation and fracture of the rim
Corrosion	Fretting wear
Osteolysis	Micro-motion of implant and presence of wear debris

the *in vivo* friction and wear of the knee joints [19,48]. Shark et al. [49,50] used a bespoke joint acoustic analysis system (JAAS) to identify the differences between an osteoarthritic knee (more AE events and higher average signal level) and a healthy knee. Advanced statistical analysis by the authors and a study by Khan and Yoho [29] showed that the AE signals could discriminate between age and progression of osteoarthritis. Rowland et al. showed that AE signals correlate well with out-of-line wear (evaluated *via* post-test surface topographies and volumetric changes) of metal-on-metal hip implants [47]. This recent progress and development of the AE technology suggest a potential tool for condition monitoring of both natural and artificial joints to diagnose joint pathologies like osteoarthritis and artificial joint failure.

The relationship between AE signals and the wear of artificial joints needs to be established to assess the potential of AE as a tool for condition monitoring of artificial joints. The difficulty with establishing this relationship is that wear of artificial joints is traditionally diagnosed during post retrieval analyses of failed implants. Since the causes of failure of implants can be related to wear and wear cannot happen without friction occurring between the articulating surfaces [36,51], an alternative is to establish a relationship between AE features and coefficient of friction to interpret the wear behaviour. The study by Patzer and Woydt [43] has shown that combining AE with the coefficient of friction tests can help improve the interpretation of wear behaviour.

The work presented in this paper is a proof-of-concept study identifying critical AE features to predict the coefficient of friction profile of simulated articulating joint replacement surfaces as a first step toward achieving the potential of AE as a tool for diagnosing orthopaedic pathologies. A bio-tribo-acoustic test methodology is used to acquire tribological and acoustic emission data synchronously. Hua, Fan and Jin used this method to correlate friction and sound pressure coefficient during bio-tribo-acoustic testing of ceramic orthopaedic biomaterials [23].

The novelty of this study lies in the use of time-dependent AE features to predict the coefficient of friction profile during bio-tribo-acoustic testing. The distribution of the different emission types from running-in to prolonged sliding stages is also investigated to understand the evolution of surface degradation. There is also a lack of adequate research on the potential of non-invasively monitoring the condition of artificial joints *via* an understanding of the tribological characteristics of the articulating joint replacement surface, highlighting the importance of this study.

Predicting the evolution of the coefficient of friction profile and monitoring surface damage of a simulated joint articulation is a significant first step toward applying the AE test method as a more dynamic and intuitive tool for monitoring the condition of orthopaedic implants.

2. Materials and Methods

2.1. Materials and Bio-Tribo-Acoustic Test Setup

A tribo-acoustic test system consisting of a tribometer and an AE

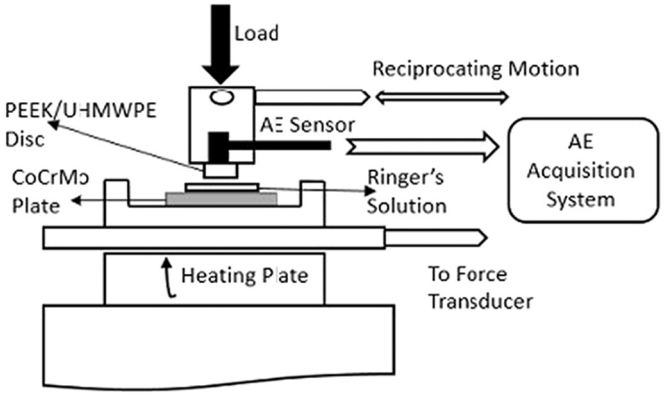

Fig. 2. Tribo-acoustic test set up comprising of a high frequency reciprocating machine and AE measurement system. The AE sensor is placed directly on the polymer specimen to reduce the effect of attenuation.

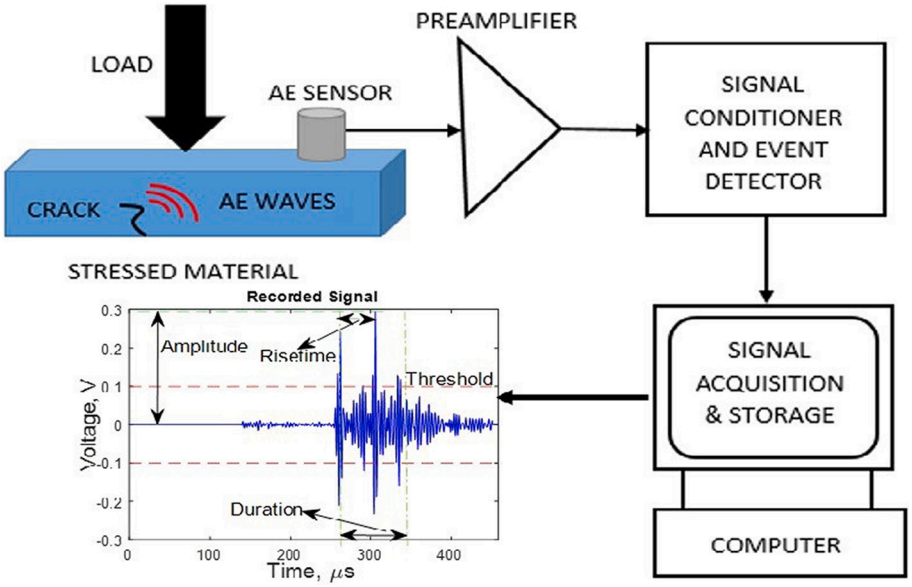

Fig. 1. Illustration of the AE test system showing progression of signal from generation to acquisition and storage. A sample signal is also shown with the basic parameters labelled.

acquisition system was designed for testing (Fig. 2). A series of tribological tests were performed to represent a metal-on-polymer joint replacement articulation surface. Reciprocating sliding tests were performed on the TE77 High-Frequency Reciprocating Machine (Phoenix Tribology, Newbury, UK) using a disc-on-plate configuration. Ultra-high-molecular-weight polyethylene (UHMWPE) discs (supplied by Penta Precision, Portsmouth, UK) were used for the reciprocating upper specimen and medical-grade cobalt chromium molybdenum alloy (CoCrMo) (machined to a surface finish of less than 0.02 μm *Ra*) on the lower fixed specimen. Poly-ether-ether-ketone (PEEK, supplied by Penta Precision, Portsmouth, UK) was chosen as an alternative material for comparison purposes. PEEK has been historically used in spinal cages and has shown promise for use in cervical TDR devices and hip implants making it a good choice of biomaterial as a comparator [35,39,54].

The PEEK and UHMWPE discs (diameter of 10 mm and 4 mm in thickness) were machined to a surface finish of 1.16 μm R_a and 3.25 μm R_a (measured with the Alicona InfiniteFocusG5 Optical 3D Measurement System from Alicona Imaging Gmbh), respectively. Since test parameters were derived using a ball and socket Charite lumbar TDR implant as the exemplar joint (see Section 2.2), a sphere-on-plane configuration was initially considered, but calculations showed that a load of about 1 N would be required on the TE77 to simulate a contact pressure that is close to that achieved in a ball-on-socket Charite lumbar TDR implant. Such a low load could make for unstable friction calculation, and, a minimum sphere diameter of 20 mm would be required, which is more than the 6 mm & 10 mm sphere diameters for the specimens used with the TE77. Hence, a disc-on-plate configuration was chosen as an alternative. The calculations can be found in Appendix A.

Polymeric test specimens were cleaned before and after each test following the method described in ASTM F732–17 [4]. The metallic specimens were washed in ethanol before and after each test. Tests were carried out at two frequencies (2 Hz and 4 Hz) for comparison purposes. There were three runs for each test condition making 12 tests in total. For each of the 12 tests, new test specimens were used.

Tests were conducted with Oxoid quarter strength Ringer's solution (supplied by a member of ThermoFisher Scientific, Oxoid Limited, Hampshire, UK) serving as the lubricating medium at a temperature of 37 ± 2 °C. The solution was prepared by dissolving one tablet in 500 ml distilled water and sterilised in an autoclave at 121 °C for 15 min. The prepared Ringer's solution was drip-fed onto the contacting surface at 0.1 ml per minute. The Ringer's solution tablet was made from sodium chloride, potassium chloride, calcium chloride $6H_2O$ and sodium bicarbonate 0.05. Temperature has also been known affect AE signals [9], but these effects are ignored since the temperature for all tests was kept constant.

2.2. Test Parameters

Hertzian contact mechanics were employed to calculate an equivalent load to be applied on the TE77 rig [25]. The maximum contact pressure is calculated based on loading and displacement conditions stated in the British Standard for wear of total intervertebral spinal disc prostheses [11], using the geometry of a ball and socket Charite lumbar TDR device (see Fig. B.15 in the appendix). The load conditions can be found in Table 2.

The maximum sliding velocity a lumbar spinal implant is subjected to during long-term wear testing on a spine simulator was calculated using simple harmonic motion equations and motion values from the BS ISO 18192-1 standard [11]. An equivalent stroke length for the TE77 was 1.0996 mm using the maximum sliding velocity (6.909 mms^{-1}) and a frequency of 2 Hz. With such a low stroke length, only fretting wear would occur, and there is an added risk of fluid entrapment due to the large diameter of the disc (10 mm). A stroke of 12.5 mm was chosen instead to obtain an average sliding velocity of 50 mm/s, which is the recommended value for a linear reciprocating wear motion in the standard for wear testing of polymeric materials used in total joint prostheses (see Annex A1 of [4]). This stroke resulted in a total sliding distance of 360 m at 0.05 ms − 1. Tests with increased frequency (4 Hz) were conducted to determine how AE features differ during severe sliding resulting in an average sliding velocity of 100 mms − 1 with a total sliding distance of 720 m at 0.1 ms − 1. A summary of all test parameters can be found in Table 3.

Table 2
Equivalent TE77 load calculated based on loading conditions in BS ISO 18192-1 [11]. Average load was chosen as test load (shown here in red font).

Load	Maximum Contact Pressure	Equivalent TE77 Load
600 N	6.5 MPa	510 N
2000 N	9.7 MPa	760 N
1300 N (average load)	8.4 MPa	660 N

2.3. AE Signal Acquisition and Analysis

An AE system consisting of a sensor, preamplifier and a PCI-2 Analogue to Digital converter from Mistras Group Inc. (Cambridge, UK) was used to acquire AE signals. A miniature Nano30 sensor (resonant frequency 300 kHz; operating range 125–750 kHz) was placed directly on the polymeric disc (Fig. 2) to detect analogue AE signals whilst reducing attenuation. These were then passed through the preamplifier (60 dB gain and frequency range of 10–900 kHz) before being converted into a digital signal by the AEWin PCI-2 card at a sampling frequency of 2 MHz. Ultrasonic gel acted as a coupling gel to ensure continuous contact between the polymer surface and the AE sensor.

AE signals from tests with zero load and no contact between specimens for three different threshold values (10, 25 and 35 dB) were analysed to assess the effect of background noise. The Fast Fourier Transform, FFT, plots (Fig. 3) show that the maximum FFT magnitude reached is lowest for tests with a 35 dB threshold setting. Hence, 35 dB was set as the amplitude threshold value for AE acquisition.

AE acquisitions were post-processed using the NOESIS Advanced Acoustic Emission Analysis Software (Mistras Group Inc. Cambridge, UK) and MATLAB for feature extraction and further statistical analysis. Feature extraction setting was kept similar to the acquisition set up apart from the threshold, which was increased to 40 dB as initial observation of the acquired signals (see Fig. B.16) shows that some systemic noise was still present in the data.

2.4. Time Series Neural Network Analysis

Artificial neural networks (ANN) are computational architectures modelled after the brain's architecture [14]. To further explore the relationship between time-dependent AE features and the coefficient of friction (CoF) profile, a nonlinear autoregressive neural network with external inputs (NARX) was deployed to predict CoF. NARX is a dynamic

Table 3
Summary of Test Parameters.

Parameter	Value (s)
Load	660 N
Frequency	2 Hz, 4 Hz
Stroke Length	12.5 mm
Sliding Velocity	50 mm/s, 100 mm/s
Test Duration	2 h
Preamplifier gain	60 dB
Threshold	35 dB
Sampling rate	2 MHz
Peak definition time (PDT)	400 μs
Hit definition time (HDT)	400 μs
Hit lockout time (HLT)	1000 μs
Maximum hit duration	1000 ms
Band pass filter	100–400 kHz

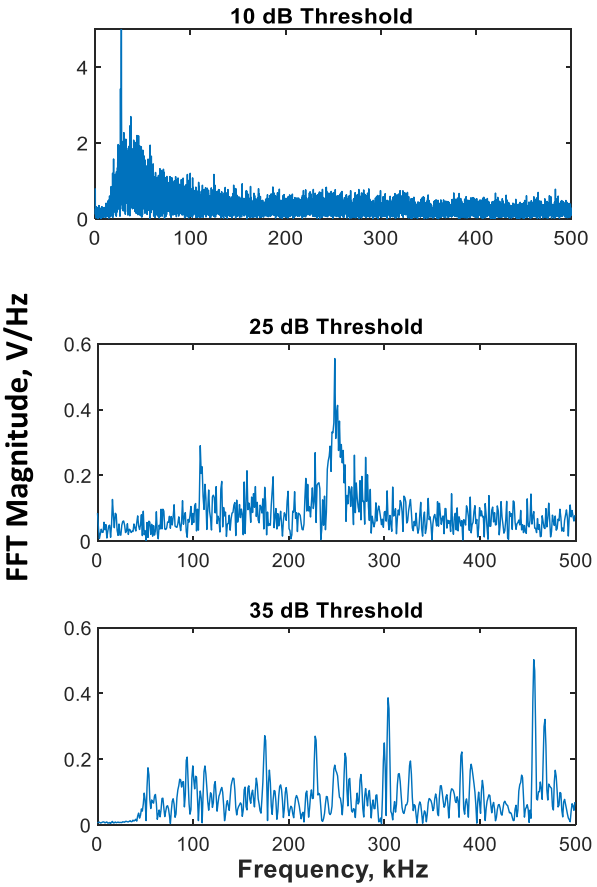

Fig. 3. Fast Fourier Transform plots of waveforms at three different threshold values. The 35 dB FFT plot has the least peak magnitude.

form of ANNs based on the linear ARX, commonly used in time series analysis [13,40,42]. It effectively solves nonlinear time series problems [42], making it suitable for this study. The NARX model equation is shown in Eq. (1), where y(t), the predicted value of the model, is predicted using its' previous values, y(t-1) to y(t-n_y), and the corresponding previous values of an external input signal, x(t-1) to x(t-n_x). There are two forms of NARX architecture: series-parallel and parallel architecture [42]. The series-parallel NARX architecture was chosen for this study because the availability of the previous values of y(t) makes the network more accurate. The Neural Net Time Series App in MATLAB version R2021a was used for training and testing the NARX models.

NARX model equation

$$y(t) = f\left(y(t-1), y(t-2), \ldots, y\left(t-n_y\right), x(t-1), x(t-2), \ldots, x(t-n_x)\right) \quad (1)$$

Herein, y(t) is the coefficient of friction recorded throughout the test and x(t) is a 3-element vector consisting of the three time-dependent AE features – absolute energy, average signal level, and AE root mean square value. The Neural Net Time Series App in MATLAB version R2021a was used for training and testing the NARX models. An illustration of the NARX network is shown in Fig. 4. There will be differences in how the two polymeric materials behave when sliding against the CoCrMo plate due to different material properties; hence, two NARX models were built - one for PEEK and the other for UHMWPE. Both models were trained using the Levenberg-Marquardt training function with ten neurons in the hidden layer. Training data were randomly divided into three splits- training data (70%), validation data (15%) and test data (15%). Performance was evaluated using mean squared error (MSE) and R^2 values. A low MSE and high R^2 value indicate good training performance.

2.5. Clustering of AE Data

Clustering is an unsupervised pattern recognition technique used to group data sets into two or more clusters based on similarities and differences noticed between the data points. This study employed the k-means clustering method. This method clusters data by minimising the sum of squared Euclidean distances from all cluster vectors to its centre [38]. In order to understand the distribution of AE signals across the two test stages, acquired hits were clustered and then categorised into one of the three emission types – burst (hits with high amplitude and short duration), continuous (hits with low amplitude and long duration) and mixed mode (mixture of burst and continuous). Since the three emission types can be distinguished using duration and amplitude values [41], they were the AE features fed into the clustering algorithm, and the initial number of k clusters was set to three emission types. The silhouette index (S.I.) plot was then used to determine if it was the optimal number of clusters.

2.6. Wear Scar Surface Analysis

Images of the worn surfaces of the polymeric specimens were obtained using an InfiniteFocusG5 Optical 3D Measurement System (supplied by Alicona Imaging Gmbh, Austria). The wear scar images of the polymeric specimens were taken at a magnification of 20× with the polariser turned off to improve the quality of the image. The pseudo colour view was selected so that regions of high height (z value) could be easily identified, enabling the identification of essential wear induced surface features that were later related to AE features.

3. Results and Discussion

3.1. Using AE to Predict the Coefficient of Friction Profile

The three time-dependent AE features: root mean square value

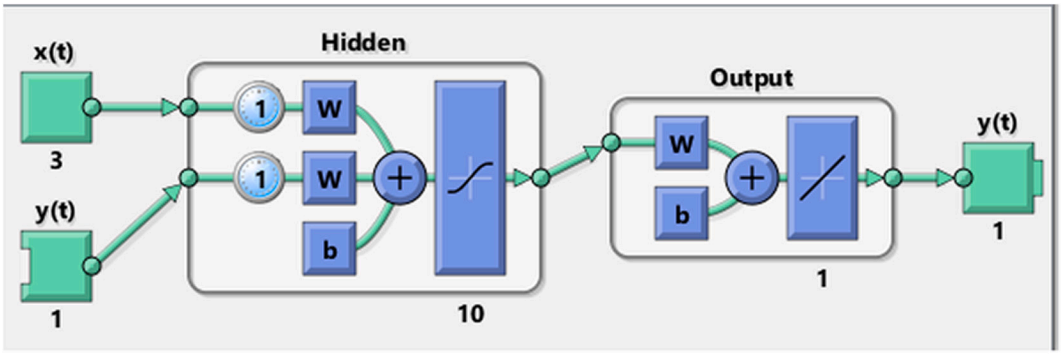

Fig. 4. NARX Neural Network. Obtained from MATLAB.

(RMS), average signal level (ASL) and absolute energy (AbsE), all exhibit similar transient responses to that of the coefficient of friction (Fig. 5 & Fig. 6) for both polymeric specimens at the two test frequencies. These trends suggest a strong potential for using time-dependent AE features to predict CoF. Other studies investigating the potential of AE as a tool for predicting tribocorrosion processes in dental implants and for the early detection of failure modes in total hip replacements also found that the coefficient of friction and absolute energy of the AE signal exhibits similar transient responses [5,30]. The predicted coefficient of friction can also be used to infer the wear behaviour of test specimens since previous studies have shown that the coefficient of friction of PEEK and UHMWPE can be directly related to wear rate [26,44].

The similar transient responses of all three time-dependent AE features to the coefficient of friction profile for both PEEK and UHMWPE (Fig. 5 & Fig. 6) make them suitable as the external input for the NARX neural network model. The training performance and training response is shown in Fig. 7 and Fig. 8.

Table 4 shows the mean square error (MSE) and R^2 values obtained after training both models. Both models have R^2 values greater than 90%, with PEEK having a slightly higher value than the UHMWPE model, implying that almost all variability is explained by both models indicating a good predictive capability. The trained network is then tested using data from the repeat bio-tribo-acoustic tests in open-loop feedback, and the results are presented in Table 5 with the training performance curves in Fig. 7: NARX Net Training Performance for PEEK (left) and UHMWPE (right)Fig. 7 and the response curves shown in Fig. 8. The test response curves are presented in Figure 9Figure 10.

The shape of the predicted CoF curve displays similar characteristics to the true curve for all tests (see Fig. 9 and Fig. 10), and the difference between predicted and actual values is low, as evidenced by the low MSE values (see Table 5). During prediction, it is assumed that the relationship between acquired AE data is uniform across all tests for each polymer at both test frequencies. Uniformity is not always guaranteed, as repeatability, however, has been a limitation of AE testing [21]. PEEK and UHMWPE have different physical and acoustic properties, such as young's modulus and attenuation coefficients affecting the characteristics of AE signals acquired from both materials. The effect of these different material properties is explained further in Section 3.4. The strain waves generated in the polymer (due to loading) would differ for each test, causing acquired AE data to have different characteristics, hence the difference between predicted and actual CoF. NARX neural net test result for UHMWPE at 2 Hz exhibited the smallest R^2 value (Table 5), and is reflected in Fig. 10, where the UHMWPE 2 Hz test curve has the most error between predicted and actual CoF values. There is a likelihood that the effect of the material and acoustic properties, in addition to the repeatability issues of AE testing, is more significant in the UHMWPE tests hence the low R^2 values obtained compared to the PEEK tests. Despite these limitations, there is still a close similarity between the predicted and actual CoF response curves (in addition to the R^2 value of about 75% obtained for UHMWPE 4 Hz test predictions), thereby supporting the hypothesis that time-dependent AE features predict the coefficient of friction profile of a metal-on-polymer joint articulation surface during *in vitro* testing. This result has promising implications for the potential use of AE testing to evaluate the frictional (and, by extension, wear) behaviour of an artificial joint bearing surface *in vivo* when it will be impossible to carry out friction and wear tests.

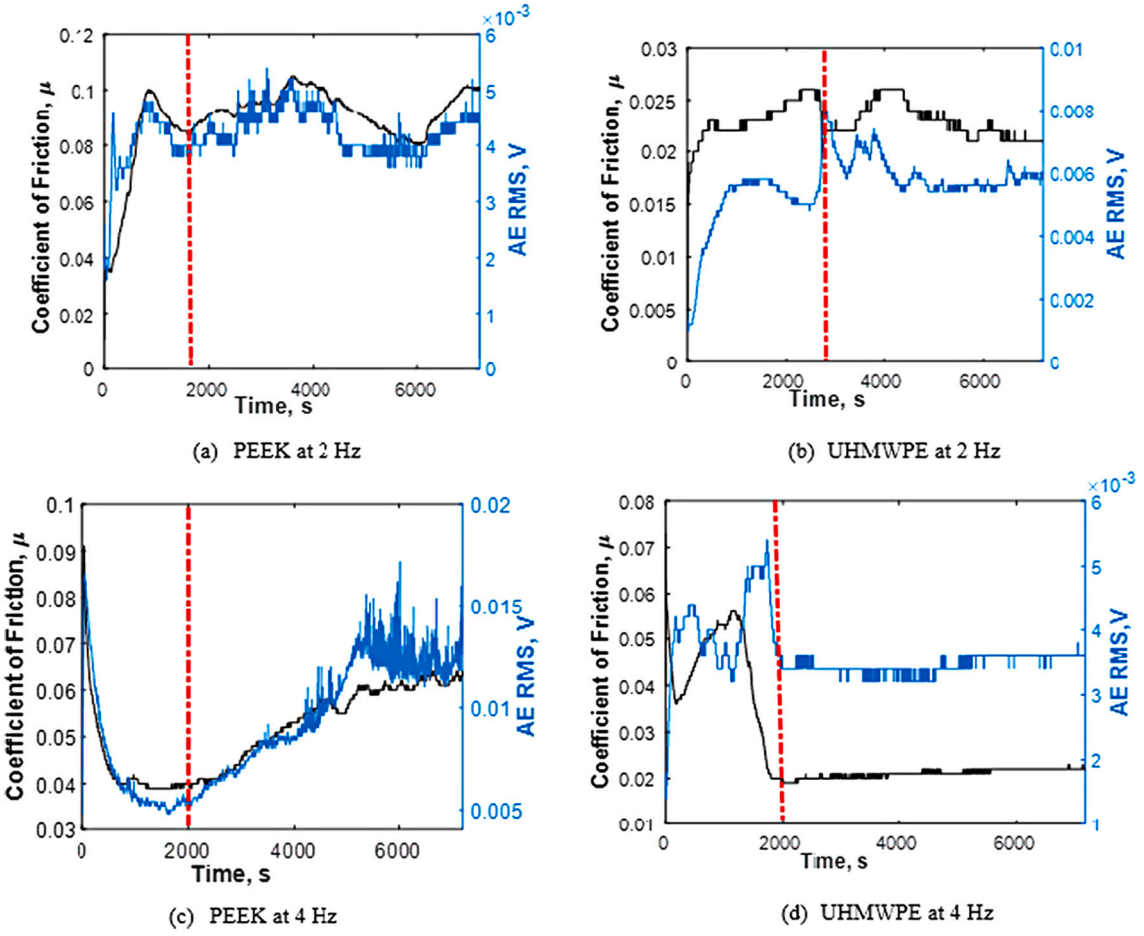

Fig. 5. RMS (blue line) & CoF (black line) plots for tests at 2 Hz and 4 Hz frequencies. Red dash line indicates transition from running-in (stage I, after lowest CoF is reached) to prolonged sliding. (For interpretation of the references to colour in this figure legend, the reader is referred to the web version of this article.)

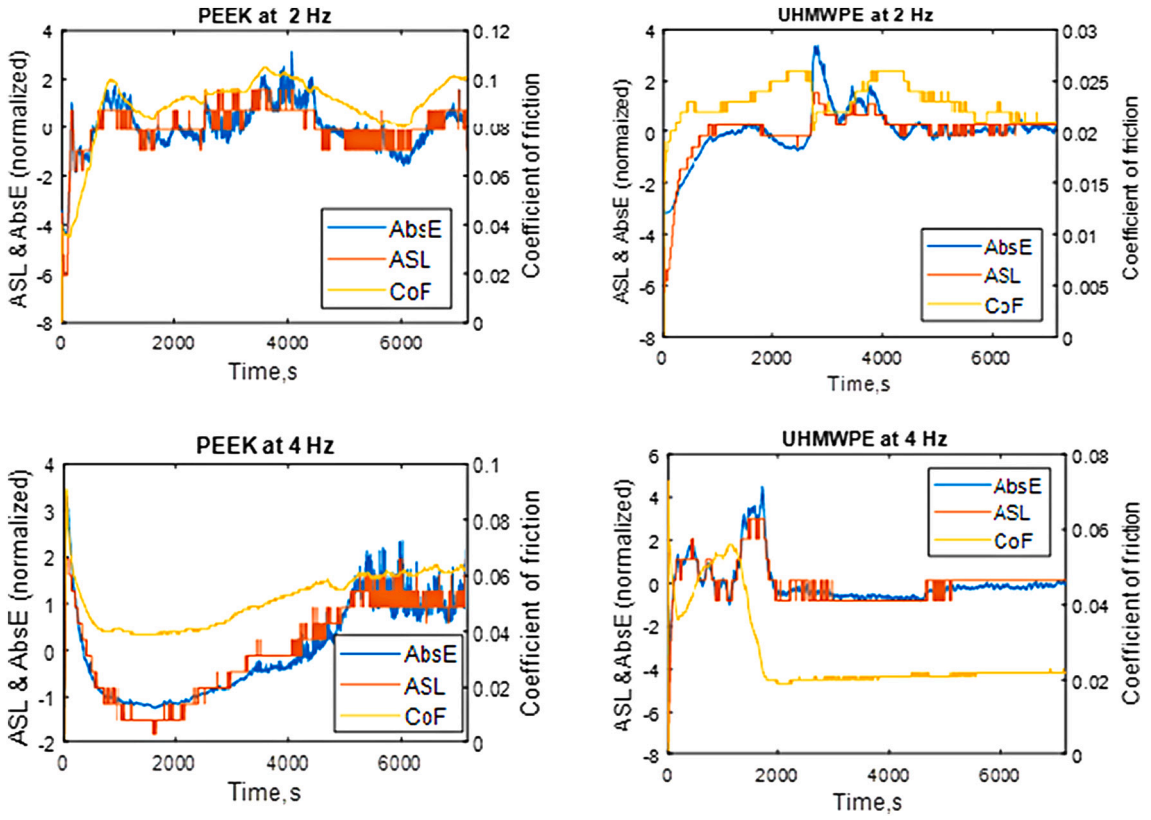

Fig. 6. Plots of average signal level (ASL) and absolute energy (AbsE) in relation to coefficient of friction (CoF).

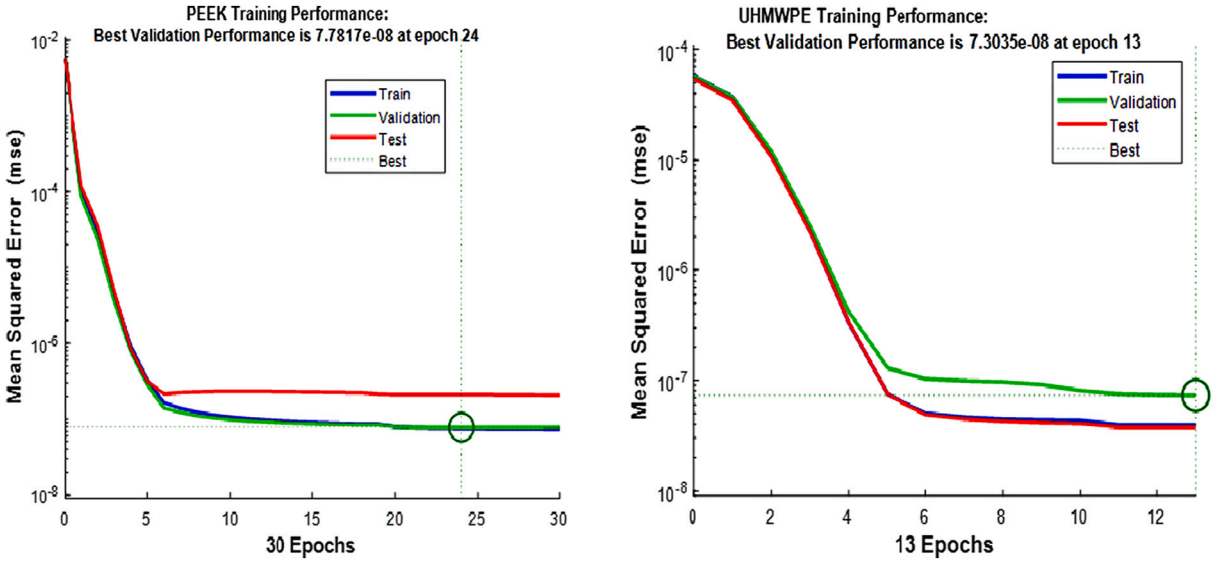

Fig. 7. NARX Net Training Performance for PEEK (left) and UHMWPE (right).

3.2. AE Parameters at Different Test Stages

The bio-tribo-acoustic tests can be split into two stages, as shown in Fig. 5. At the onset of sliding, CoF and RMS values are seen first to reach an initial maximum followed by a minimum. This initial increase is due to the collision of surface asperities at the onset of sliding, also known as the running-in stage [7]. The source of AE signals during running-in is the energy released during the initial collision and subsequent fracture of asperities, and the material deformation and crack formation that occurs within the contact region [6]. Stage 2 is where prolonged sliding occurs, as observed by the continued variation in CoF and RMS values. These variations are less severe than during running-in, indicating a slight change in friction over a significant period. Continued plastic deformation and crack propagation as sliding progresses is the predominant source of AE at this stage. There is also the ploughing action of deformed asperities (for the UHMWPE specimens) and the presence of wear particles entrapped within the contacting surfaces (for the PEEK specimens) [24], hence the variation in underlying tribological processes and the recorded CoF and RMS values.

K-means clustering was used to understand better the distribution of

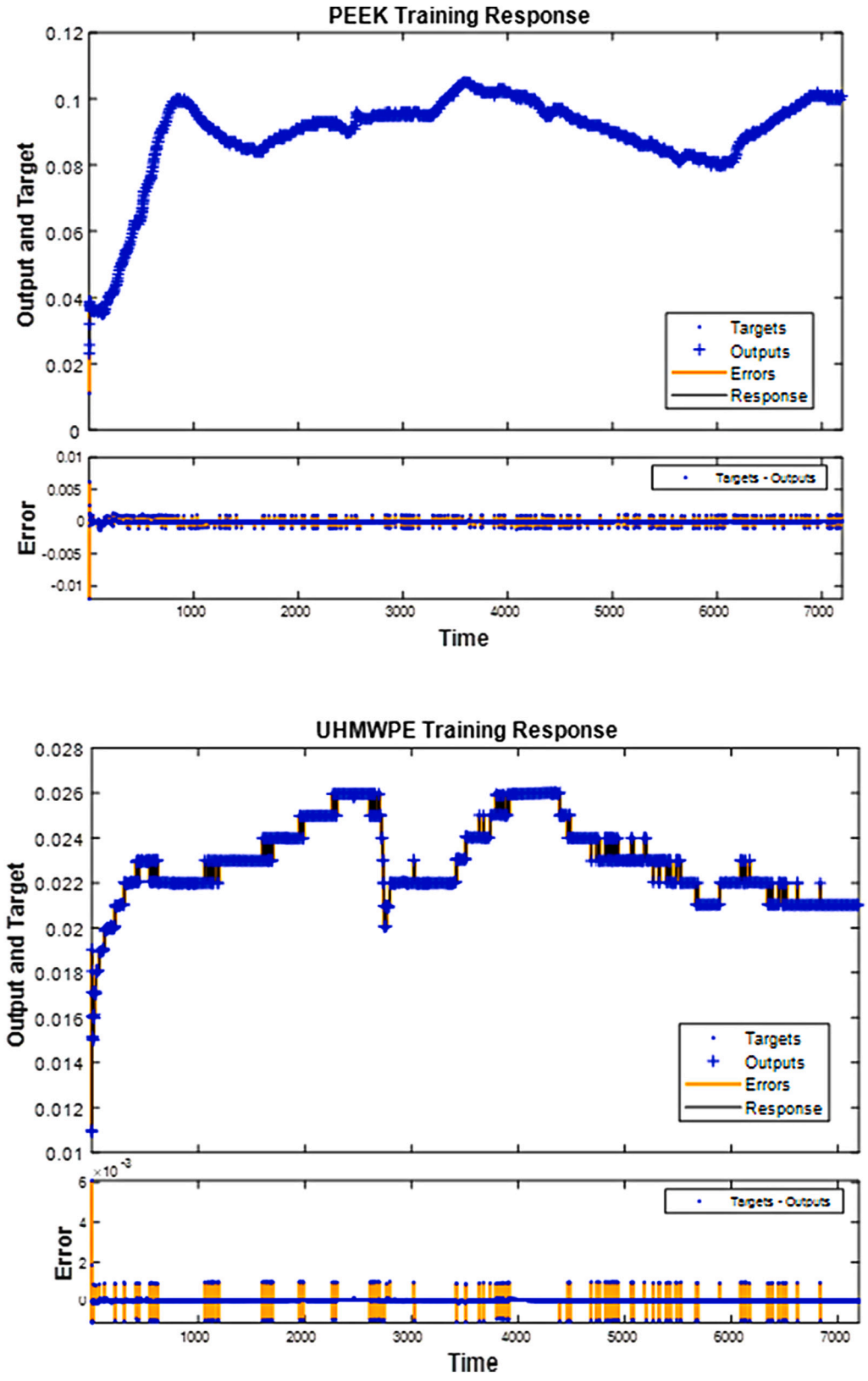

Fig. 8. NARX Net Training Response for PEEK (top) and UHMWPE (bottom).

AE signals across the two test stages and to cluster and categorise AE signals into one of the three emission types. The silhouette index plots affirmed the choice of three clusters (Fig. 11), where most of the hits in all three clusters had silhouette values greater than 70%, proving that they belong to those clusters. It was assumed that the misclassified hits (hits with negative silhouette values) do not significantly affect the clustering results due to their small number. Cluster assignments for both polymeric materials at frequencies 2 Hz and 4 Hz are shown using the duration *vs* amplitude plots in Fig. 12. After post-processing of AE signals, the UHMWPE 2 Hz tests had more minor hits than the other tests

Table 4
NARX Neural Network Training Result Summary.

	PEEK	UHMWPE
MSE	7.78×10^{-8}	7.30×10^{-8}
R^2 value	0.9995	0.9858

Table 5
A summary of CoF prediction results with test data.

	PEEK		UHMWPE	
	2 Hz	4 Hz	2 Hz	4 Hz
MSE	6.78×10^{-5}	6.39×10^{-7}	0.0011	1.08×10^{-6}
Regression, R	0.9718	0.9979	0.5976	0.8691
Mean CoF (Predicted) ± Standard Deviation	0.1079 ± 0.0150	0.0510 ± 0.0088	0.0251 ± 0.0062	0.0190 ± 0.0017
Mean CoF (Actual) ± Standard Deviation	0.1128 ± 0.0202	0.0513 ± 0.0093	0.0436 ± 0.0312	0.0187 ± 0.0020

hence why their clusters are not as densely packed as the other tests.

Each cluster has similar properties for both materials at the two test frequencies. Based on observation of the cluster properties in conjunction with the features of the three emission types, the clusters are labelled as follows:

- Burst Emission – Clusters with high amplitude and short duration hits. These are in cluster 3 for the PEEK 2 Hz tests, cluster 2 for the PEEK 4 Hz tests, cluster 2 for the UHMWPE 2 Hz tests and cluster 1 for the UHMWPE 4 Hz tests.
- Continuous Emission – Clusters with low amplitude and long duration hits. These correspond to cluster 2 in PEEK 2 Hz tests and cluster 3 in PEEK 4 Hz, UHMWPE 2 Hz & UHMWPE 4 Hz tests.
- Mixed Emission – Clusters with mid-range amplitude and short to medium duration hits. These correspond to cluster 1 in PEEK 2 Hz, PEEK 4 Hz & UHMWPE 2 Hz tests and cluster 2 in UHMWPE 4 Hz tests.

The example waveform of each emission type is presented in Fig. B.18.

In addition to duration and amplitude, the peak frequency values exhibit significant differences for each emission type, as shown in Tables 6, 7, 8 and 9, where the mean value and 95% confidence interval (C. I.) of the three AE features are presented.

Fig. 13 shows the distribution of AE signal types across the two test stages for PEEK and UHMWPE at both test frequencies. All emission types are present in both test stages but different proportions. Most of the burst emissions are present in stage I (*i.e.*, running-in) of the PEEK 2 Hz tests (see Fig. 12a), whilst a higher percentage of the continuous emissions are present in stage II (*i.e.*, prolonged sliding) for all tests. Burst emissions are generated due to damage formation, such as asperity fractures [3,53]. Since micro-crack formations characterise the running-in stage due to contact and fracture of asperities at the onset of sliding, which would cause an immediate release of high strain energy, it is no surprise that a higher percentage of the burst emissions are present

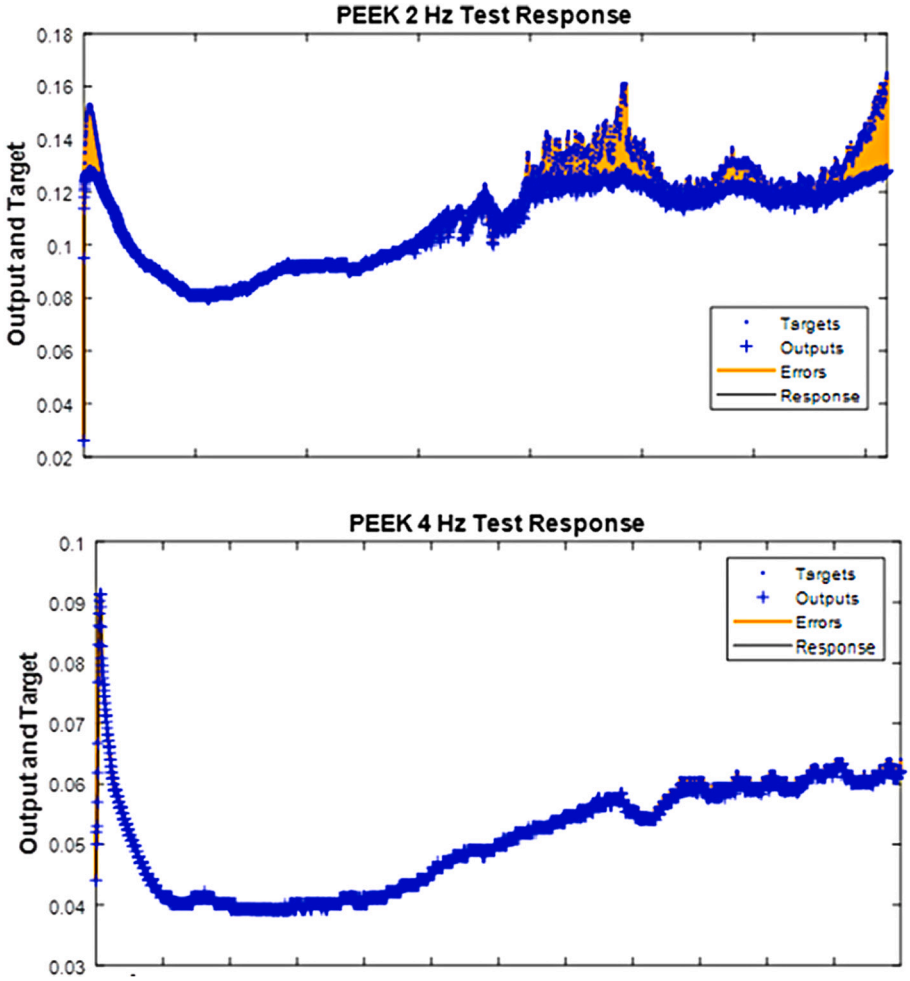

Fig. 9. Test Response for PEEK Tests at 2 Hz (top) and 4 Hz (bottom).

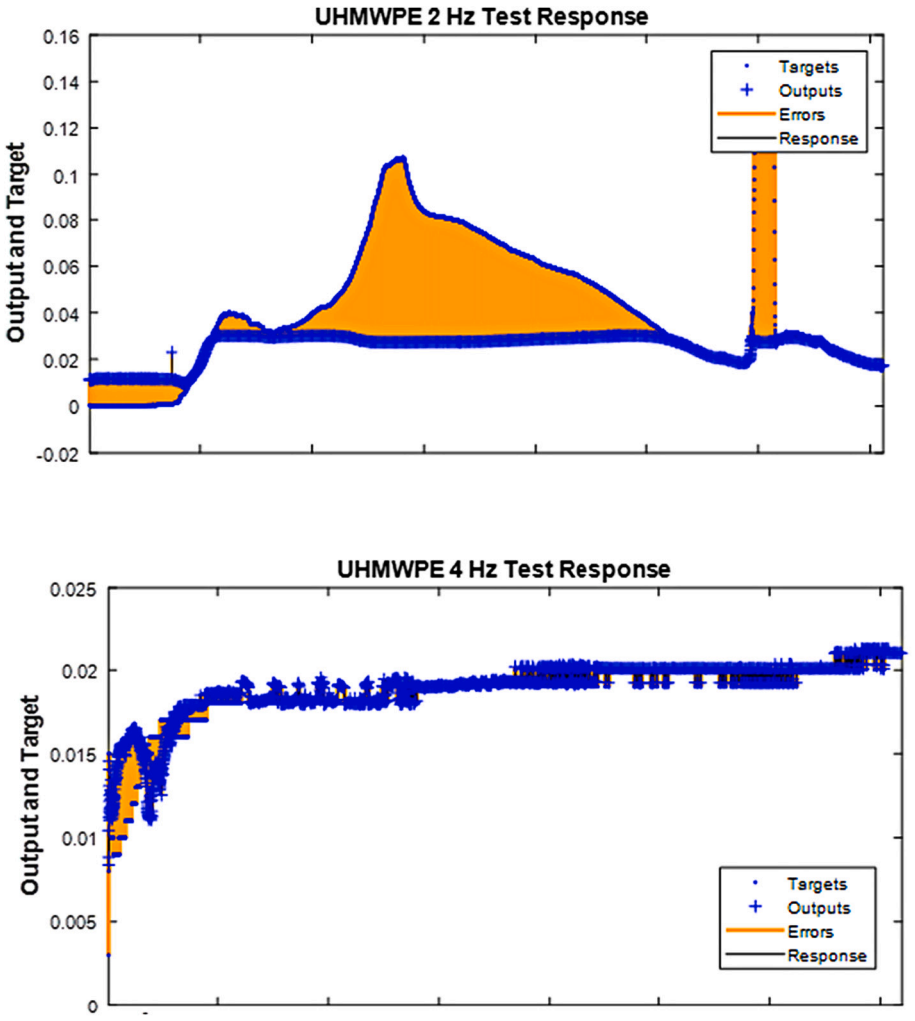

Fig. 10. Test Response Curves for UHMWPE Tests at 2 Hz (top) and 4 Hz (bottom).

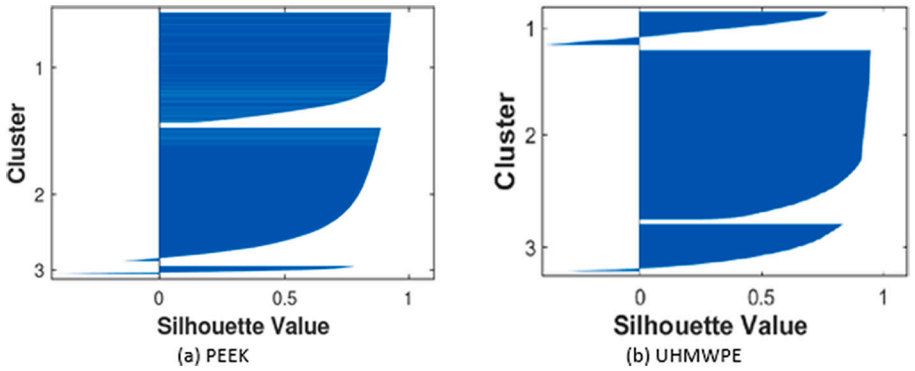

Fig. 11. Silhouette plot showing silhouette values of hits in each cluster.

during this stage of the PEEK 2 Hz tests. The force required to separate adhered particles or junctions as sliding progresses is another source of burst emissions during running-in.

Unlike the PEEK 2 Hz tests, a higher percentage of burst emissions were generated during the prolonged sliding stage, not the running-in stage as expected. These signals are due to ploughing causing either deformed asperities during UHMWPE/CoCrMo tests [32] or the generation of wear debris during PEEK/CoCrMo tests [52]. Both wear processes cause the release of sudden, instantaneous strain energy, thereby generating burst emissions. The definition of tribological processes softens when mixed emissions are measured, where both burst and continuous emissions cannot always be isolated. The most common is for them to coincide, thereby generating mixed emissions.

The commonality between all tests is the higher percentage of the continuous emissions present in the prolonged sliding stage. Continuous emissions are generated when multiple signals overlap, making them indistinguishable, and the envelope of the signal amplitudes becomes constant [3,53]. These emissions are predominantly steady friction and

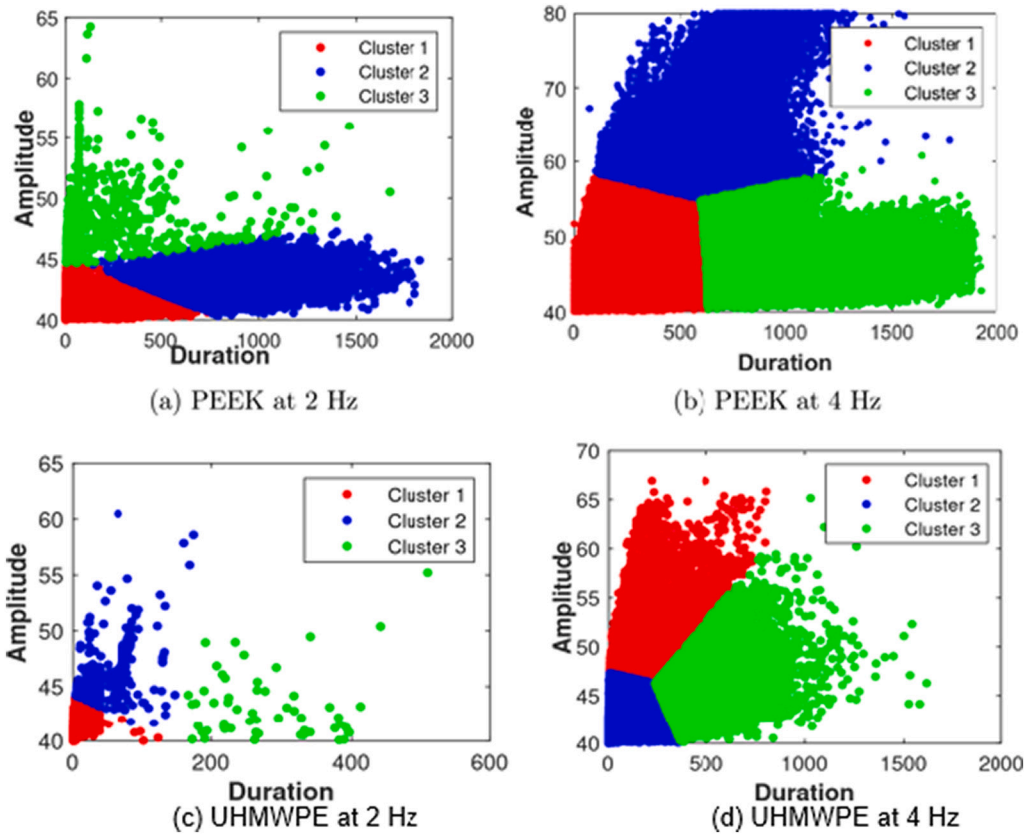

Fig. 12. Cluster Assignments.

Table 6
Mean and 95% confidence intervals (C.I.) of AE features in each cluster for PEEK at 2 Hz (Fig. 12a).

AE Feature	Burst (Cluster 3)		Mixed (Cluster 1)		Continuous (Cluster 2)	
	Mean	C.I.	Mean	C.I.	Mean	C.I.
Duration, μs	208.73	187.92, 231.52	112.10	108.24, 115.27	901.20	896.32, 905.91
Amplitude, dB	48.22	48.05, 48.50	41.06	41.04, 41.08	43.11	43.09, 43.13
Peak Frequency, kHz	260.31	258.05, 262.21	222.82	221.71, 223.88	218.96	217.98, 219.89

Table 7
Mean and 95% confidence intervals (C.I.) of AE features in each cluster for PEEK at 4 Hz (Fig. 12b).

AE Feature	Burst (Cluster 2)		Mixed (Cluster 1)		Continuous (Cluster 3)	
	Mean	C.I.	Mean	C.I.	Mean	C.I.
Duration, μs	679.61	676.57, 682.22	100.99	100.20, 101.76	1134.9	1132.37, 1137.16
Amplitude, dB	67.83	67.73, 67.92	44.87	44.85, 44.89	45.69	45.66, 45.72
Peak Frequency, kHz	238.58	238.14, 239.00	246.28	246.15, 246.40	240.23	240.00, 240.46

Table 8
Mean and 95% confidence intervals (C.I.) of AE features in each cluster for UHMWPE at 2 Hz (Fig. 12c).

AE Feature	Burst (Cluster 2)		Mixed (Cluster 1)		Continuous (Cluster 3)	
	Mean	C.I.	Mean	C.I.	Mean	C.I.
Duration, μs	50.78	48.71, 52.91	3.88	3.62, 4.18	282.47	263.05, 306.03
Amplitude, dB	45.84	45.71, 46.00	41.15	41.11, 41.20	43.55	42.87, 44.51
Peak Frequency, kHz	231.45	230.14, 232.59	210.96	209.53, 212.56	218.99	209.02, 229.22

Table 9
Mean and 95% confidence intervals (C.I.) of AE features in each cluster for UHMWPE at 4 Hz (Fig. 12d).

AE Feature	Burst (Cluster 1)		Mixed (Cluster 2)		Continuous (Cluster 3)	
	Mean	C.I.	Mean	C.I.	Mean	C.I.
Duration, μs	154.68	151.66, 157.79	42.94	42.33, 43.63	503.98	500.81, 506.92
Amplitude, dB	51.24	51.15, 51.33	42.63	42.61, 42.65	46.04	45.99, 46.09
Peak Frequency, kHz	219.34	218.69, 220.03	214.49	214.04, 214.89	229.07	228.79, 229.32

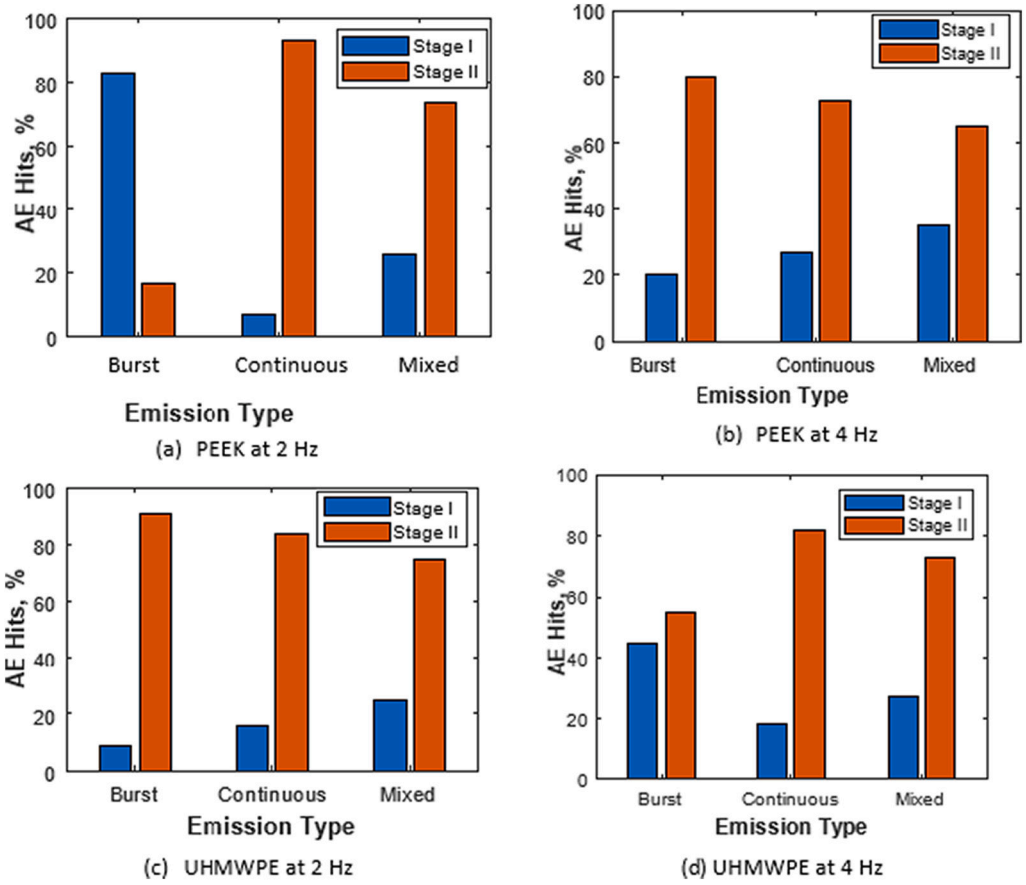

Fig. 13. Distribution of AE signals across test stages.

plastic deformation of surface asperities, mainly during prolonged sliding.

The two test stages can be related to the everyday motion of the natural and artificial joints, with the running-in stage representative of the static friction expected at the start of a movement (*e.g.*, starting to stand), during which a more significant amount of force would be exerted whilst the prolonged sliding stage is representative of the period of the actual motion (*e.g.*, walking).

The above findings suggest that frictional events and plastic deformation that generates continuous emissions can be vital for monitoring the tribological behaviour of two contacting surfaces during sliding. The distribution of continuous emissions identifies test stages and, by extension, the most dominant surface damage occurring.

3.3. AE and Wear

The wear mechanism experienced by the test specimens is predominantly adhesive with a polymer sliding against a smooth metal surface [6], confirmed by wear scar imaging (see Fig. 14), whereby the peak regions (regions with high z value), presenting in the centre of the contact zone, indicate where adhesion has taken place. Studies have shown that the frequency of AE signals can also be used to infer wear behaviour [18]. It has been reported that the AE frequency spectra due to sliding friction have a frequency band of 50 to 250 kHz [18], and the majority of hits from these tests had peak frequencies in the range of 150 to 275 kHz (Fig. 15) proving that sliding friction is the most dominant source of detected AE hits. This effect is further evidenced by the fact that continuous emission hits, known to be primarily due to sliding friction, have average peak frequencies in the range of 220 to 240 kHz (see Table 6 to Table 9).

3.4. Effect of Differing Material Properties

It was observed that the PEEK tests produced more AE hits with higher intensities than the UHMWPE tests, which can be attributed to their different mechanical properties, which govern their sliding characteristics. PEEK has a higher young's modulus and ultimate tensile strength than UHMWPE, making it more resistant to deflection and plastic deformation. The same load would require more force to break PEEK asperities than those on the UHMWPE surface, generating more strain energy at the contact zone and producing AE hits with a higher intensity and more hits overall. These trends are in line with the study by Belyi et al. [6] where it was found that AE intensity is higher for polymers with a higher Young's modulus.

Other factors that could explain the differences are the attenuation coefficient and speed of sound in both materials. Although the attenuation coefficient of PEEK (0.38 dB/mm) is higher than that of UHMWPE (0.24 dB/mm), sound moves faster in PEEK (2555 m/s) than in UHMWPE (1950 m/s) [12]. The low speed of sound coupled with the higher deformability of UHMWPE could lead to more loss of signal levels as it travels from the source to the sensor, which explains why AE signals from UHMWPE have less intensity than AE signals from PEEK.

It is worth noting that despite the difference in intensity levels, AE signals from both materials behave similarly, showing that differing material properties only affect the intensity of the signal. AE signals can infer bio-tribological characteristics irrespective of the material type.

3.5. Clinical Usability

Further research is currently being carried out to fully realise the potential of AE as a biotribological diagnostic tool. One immediate concern for using AE *in vivo* is the possible attenuation of signals due to

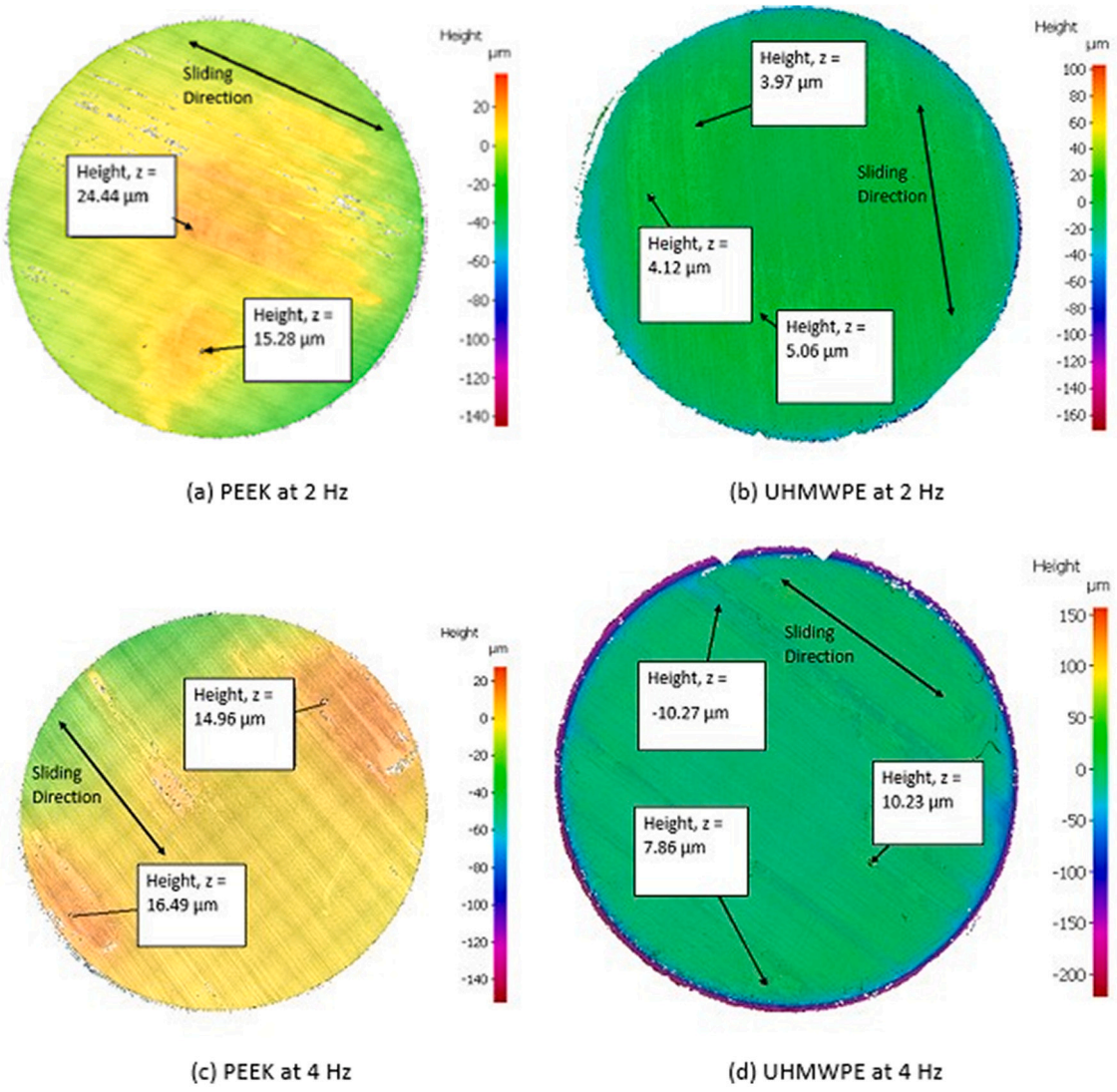

Fig. 14. Polymeric specimens wear scar images (regions of high z value indicate adhesion).

soft tissue around the joints. Khan-Edmundson et al. investigated this and found that the maximum frequency at the skin surface is approximately 20 kHz [28]. Using a similar approach to study the attenuation characteristics of total disc replacement devices can be helpful in the interpretation of *in vivo* test results. Rodgers et al. also compared *in vivo* and *in vitro* testing of total hip arthroplasty implants and found that although tissue attenuation caused a reduction in the magnitude of the signal for the *in vivo* tests, the characteristic frequencies were similar in both cases [46], highlighting the influence of attenuation is at a minimum.

Although tests reported in this study are based on TDR devices, with some modifications, the technique could be applied to other artificial joints, such as hip and knee joint replacements, which is an exciting development for the monitoring of artificial joints.

3.6. Limitations of the Study

These results suggest an enormous potential for AE as a tool for monitoring artificial joint tribological behaviour. Still, it isn't without its' limitations. Further development work should now seek to better replicate the complex kinematics of a range of joint prostheses - either with bench test geometries closer to the devices or with actual implants. Exploration of the effects of wear throughout the device's lifetime would also be a further step toward a condition monitoring system. Further development of machine learning techniques and high-order analysis to observe the relationship between AE features and simulated damage modes may reveal additional insights. Ultimately, the method will require a transition from *in-vitro* to *in-vivo* and, in doing so, refinement of signal acquisition techniques, data processing and analysis.

4. Conclusions

In being able to successfully predict and interpret frictional processes in a representative metal-on-polymer articulating joint (during *in vitro* testing), this study has demonstrated the capability of the AE technique as a tool for understanding the tribological behaviour of an artificial joint *in vivo*.

The following conclusions are reached.

- Using a NARX neural network, time-dependent AE features can predict the CoF profile with an R^2 value of over 90%.
- The percentage of continuous emissions generated is significant for identifying the test stage and inferring surface damage evolution.
- Differing biomaterial properties would not affect the biotribological interpretations of the signals generated.

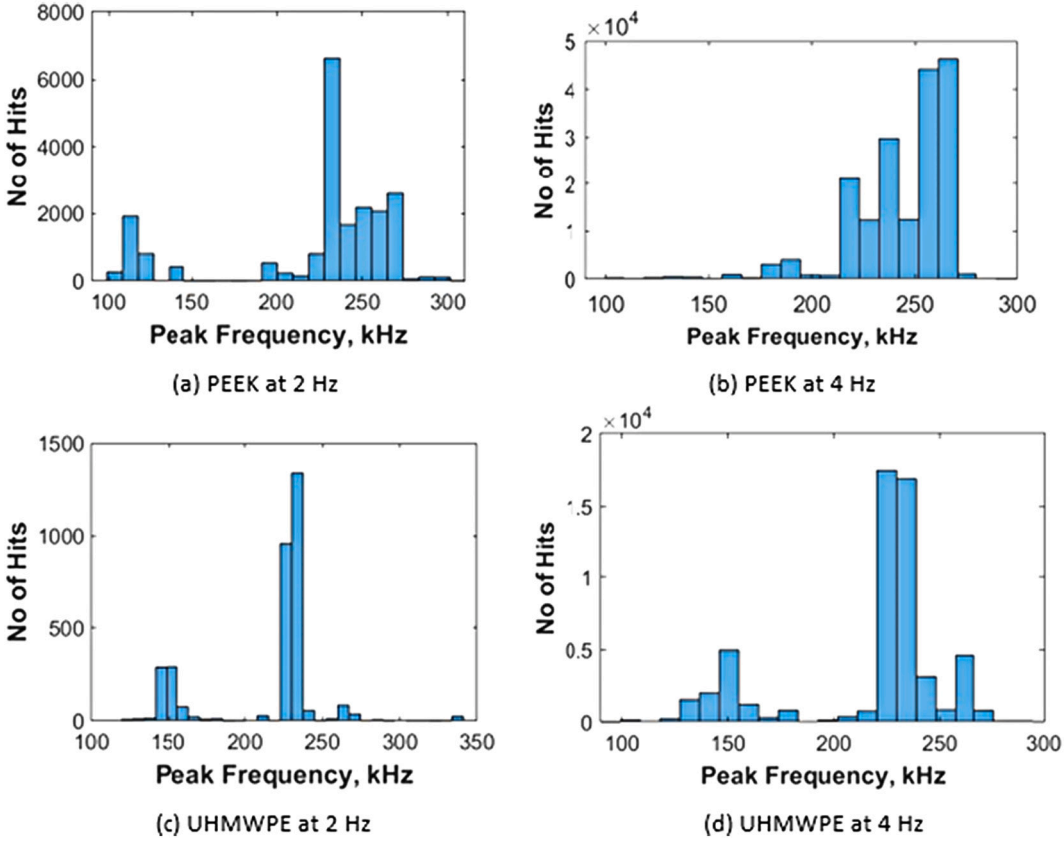

Fig. 15. Peak Frequency Distribution Plots.

The ability to relate AE features to the evolution of wear and frictional processes provides a more intuitive and dynamic process of monitoring the tribological conditions of artificial joints, significantly impacting both patients and the healthcare industry – reducing exposure to radiation for patients and cost for healthcare institutes.

Declaration of Competing Interest

The authors declare that they have no known competing financial interests or personal relationships that could have appeared to influence the work reported in this paper.

Data availability

Data will be made available on request.

Acknowledgment

This study is supported by the University of Birmingham, School of Engineering PhD Scholarship. The experimental equipment used in this research, within the Birmingham Centre for Cryogenic Energy Storage, was obtained with support from the Engineering and Physical Sciences Research Council, under the "eight great technologies: energy storage theme" (grant numbers EP/L017725/1 and EP/R041407/1).

Appendix A. Test Geometry Determination

At a maximum possible load of 2000 N [11], the maximum contact pressure of a ball and socket Charite Lumbar Spinal Implant (with ball radius 14 mm and clearance of 0.35 mm [37] was calculated to be 9.7 MPa and a contact area radius of 9.91 mm using Hertzian contact mechanics [25]. The load and corresponding contact area radius required to achieve an equivalent contact pressure on the TE77 for a sphere-on-plane configuration can be found in Table A.10. A 20 mm diameter (and above) sphere is required to simulate a close enough maximum contact pressure on the TE77 and this is more than the 6 mm & 10 mm diameter ball the TE77 is configured for. Also, the resulting contact area radius simulated is much lower than that of the Charite Lumbar Spinal Implant bearing surface. Moreover, such a low load could make the friction calculation unstable. For these reasons, a disc-on-plate configuration was decided upon.

Table A.10
Load and Contact Mechanics for a TE77 sphere-on-plane configuration.

Sphere Diameter, mm	Force, N	Maximum Contact Pressure, MPa	Contact Area Radius, mm
6	1	25.6	0.137
10	1	18.2	0.162
20	1	11.5	0.204

Appendix B. Additional Figures

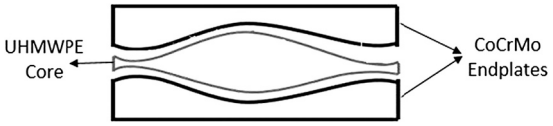

Fig. B.16. Charite Implant Schematic. The Charite Implant was used to derive test parameters. UHMWPE core has a radius ranging from 10 mm to 14 mm and a clearance of 0.35 mm between the core and the endplates.

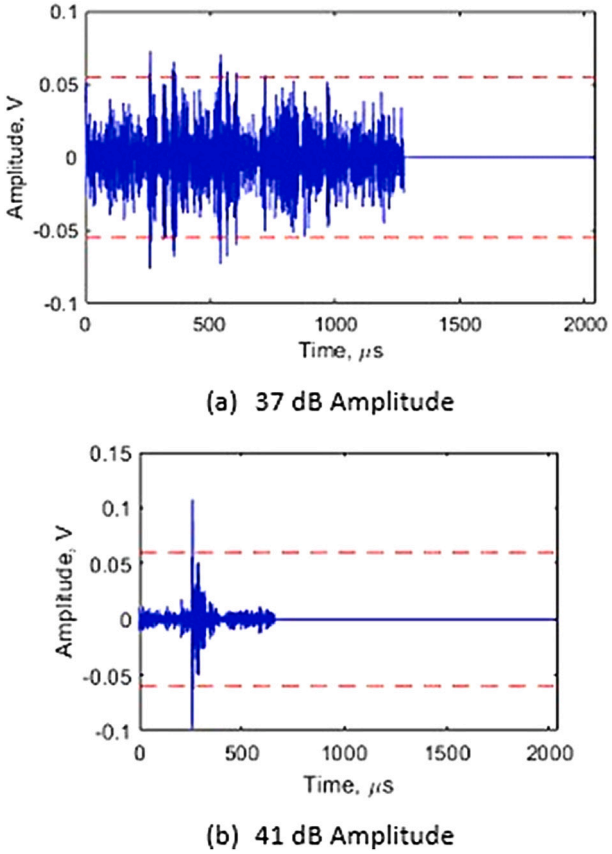

Fig. B.17. Raw AE signal at (a) 37 dB and (b) 41 dB amplitudes. The 37 dB signal is noisier than the 41 dB signal.

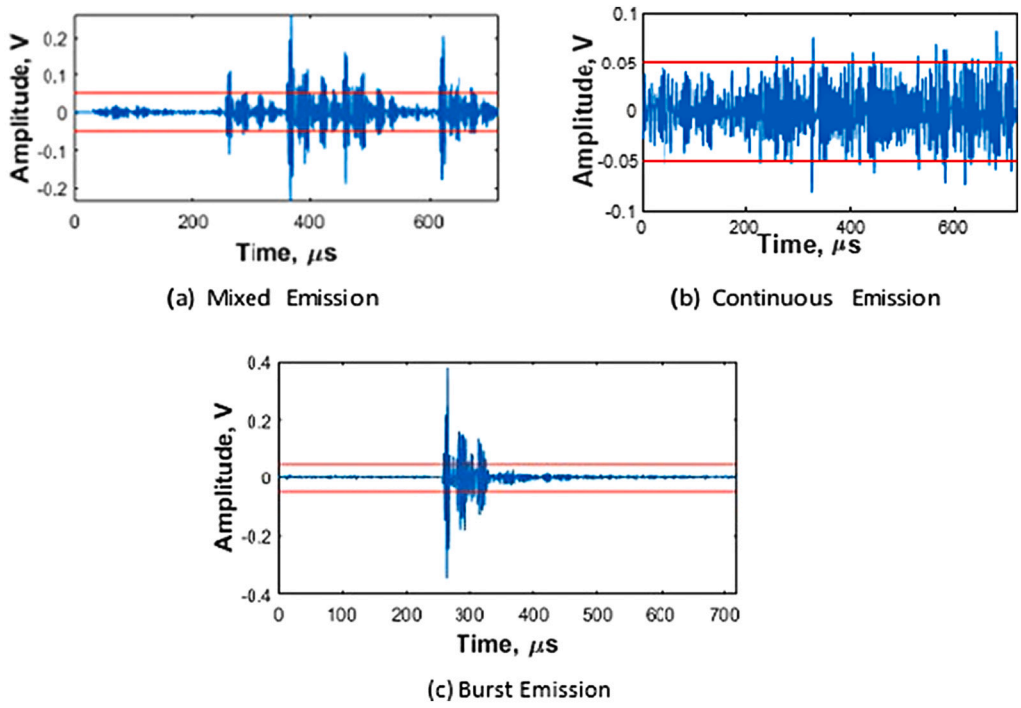

Fig. B.18. Waveform plot of each emission type (red line indicates amplitude threshold). (For interpretation of the references to colour in this figure legend, the reader is referred to the web version of this article.)

References

[1] Y. Abu-Amer, I. Darwech, J.C. Clohisy, Aseptic loosening of total joint replacements: mechanisms underlying osteolysis and potential therapies, Arth. Res. Ther. 9 (SUPPL.1) (2007) 1–7, https://doi.org/10.1186/ar2170.

[2] S. Agcaoglu, O. Akkus, Acoustic emission based monitoring of the microdamage evolution during fatigue of human cortical bone, J. Biomech. Eng. 135 (8) (2013) 081005, https://doi.org/10.1115/1.4024134.

[3] K. Asamene, M. Sundaresan, Analysis of experimentally generated friction related acoustic emission signals, Wear 296 (2012) 607–618, https://doi.org/10.1016/j.wear.2012.07.019. Elsevier.

[4] ASTM International, F732–17(2017) Standard Test Method for Wear Testing of Polymeric Materials Used in Total Joint Prostheses, United States, ASTM International, 2017, https://doi.org/10.1520/F0732-17.

[5] V.A.R. Barão, et al., Prediction of tribocorrosion processes in titanium-based dental implants using acoustic emission technique: initial outcome, Mater. Sci. Eng. C 123 (February) (2021), https://doi.org/10.1016/j.msec.2021.112000.

[6] V.A. Belyi, O.V. Kholodilov, A.I. Sviridyonok, Acoustic spectrometry as used for the evaluation of tribological systems, Wear 69 (1981) 309–319.

[7] R.J. Boness, S.L. McBride, Adhesive and abrasive wear studies using acoustic emission techniques, Wear 149 (1991) 41–53.

[8] R. Boness, S.L. McBride, M. Sobczyk, Wear studies using acoustic emission techniques, Tribol. Int. 23 (5) (1990) 291–295, https://doi.org/10.1016/0301-679X(90)90001-6.

[9] M.J.G.N. Boon, et al., Temperature and load effects on acoustic emission signals for structural health monitoring applications, in: 7th European Workshop on Structural Health Monitoring, EWSHM 2014 - 2nd European Conference of the Prognostics and Health Management (PHM) Society, 2014, pp. 1997–2003.

[10] T. Brown, et al., An in vitro assessment of wear particulate generated from nubac: a peek-on-peek articulating nucleus replacement device: methodology and results from a series of wear tests using different motion profiles, test frequencies, and environmental conditions, Spine 36 (26) (2011) 1675–1685, https://doi.org/10.1097/BRS.0b013e31821ac8a0.

[11] BS ISO 18192-1, BSI Standards Publication Implants for Surgery — Wear of Total Intervertebral Spinal Disc Prostheses Part 1 : Loading and Displacement Parameters for Wear Testing and Corresponding Environmental Conditions for Test, 2011.

[12] C. Cadot, J.-F. Saillant, B. Dulmet, Method for acoustic characterization of materials in temperature, Wcndt 2016 (2016) 1–9.

[13] S. Chen, S.A. Billings, P.M. Grant, Non-Linear Systems Identification Using Neural Networks, Research Report. Acse Report 370. Sheffield. Available at, https://eprints.whiterose.ac.uk/78225/, 1989.

[14] B. Curry, D.E. Rumelhart, MSnet: a neural network which classifies mass spectra, Tetrahedron Comput. Methodol. 3 (3–4) (1990) 213–237, https://doi.org/10.1016/0898-5529(90)90053-B.

[15] T. David, Long-term results of one-level lumbar arthroplasty: minimum 10-year follow-up of the CHARITÉ artificial disc in 106 patients, Spine 32 (6) (2007) 661–666, https://doi.org/10.1097/01.brs.0000257554.67505.45.

[16] C.J. Devin, T.G. Myers, J.D. Kang, Chronic failure of a lumbar total disc replacement with osteolysis: report of a case with nineteen-year follow-up, J. Bone Joint Surg. Ser. A 90 (10) (2008) 2230–2234, https://doi.org/10.2106/JBJS.G.01712.

[17] D.G. Eckold, K.D. Dearn, D.E.T. Shepherd, The evolution of polymer wear debris from total disc arthroplasty, Biotribology 1–2 (2015) 42–50, https://doi.org/10.1016/j.biotri.2015.04.002. Elsevier Ltd.

[18] C. Ferrer, et al., Discrete acoustic emission waves during stick-slip friction between steel samples, Tribol. Int. 43 (1–2) (2010) 1–6, https://doi.org/10.1016/j.triboint.2009.02.009. Elsevier.

[19] R.P. Franke, et al., Acoustic emission measurement system for the orthopedical diagnostics of the human femur and knee joint, J. Acoust. Emission 22 (2004) 236–242.

[20] A. Hase, H. Mishina, M. Wada, Microscopic study on the relationship between AE signal and wear amount, Wear 308 (2013) 142–147, https://doi.org/10.1016/j.wear.2013.08.005. Elsevier.

[21] C.J. Hellier, Chapter 10: Acoustic emission testing, in: Handbook of Nondestructive Evaluation, The McGraw-Hill Companies, Inc, Boston, 2003, pp. 10.1–10.39.

[22] T.J. Hoskins, et al., Acoustic noise from polymer gears – a tribological investigation, Mater. Des. 32 (6) (2011) 3509–3515, https://doi.org/10.1016/j.matdes.2011.02.041. Elsevier Ltd.

[23] Z. Hua, Y. Fan, Z. Jin, A biotribo-acoustic testing method for ceramic orthopaedic biomaterials, Tribol. Int. 71 (2014) 1–6, https://doi.org/10.1016/j.triboint.2013.10.015. Elsevier.

[24] C.L. Jiaa, D.A. Dornfeld, Experimental studies of sliding friction and wear via acoustic emission signal analysis, Wear 39 (1990).

[25] K.L. Johnson, Contact Mechanics, Cambridge University Press, Cambridge, 1985.

[26] K.S. Kanaga Karuppiah, et al., Friction and wear behavior of ultra-high molecular weight polyethylene as a function of polymer crystallinity, Acta Biomater. 4 (5) (2008) 1401–1410, https://doi.org/10.1016/j.actbio.2008.02.022.

[27] K. Karl, Tribology and total hip arthroplasty implants, Orthopedics 36 (11) (2013) 854–855, https://doi.org/10.3928/01477447-20131021-05.

[28] A. Khan-Edmundson, et al., Tissue attenuation characteristics of acoustic emission signals for wear and degradation of total hip arthroplasty implants, in: IFAC Proceedings Volumes (IFAC-PapersOnline), IFAC, 2012, pp. 355–360, https://doi.org/10.3182/20120829-3-HU-2029.00046.

[29] T.I. Khan, H. Yoho, Integrity analysis of knee joint by acoustic emission technique, J. Multimodal User Interfaces 10 (4) (2016) 319–324, https://doi.org/10.1007/s12193-015-0206-3. Springer Berlin Heidelberg.

[30] C. Lee, et al., Non-invasive early detection of failure modes in total hip replacements (THR) via acoustic emission (AE), J. Mech. Behav. Biomed. Mater. 118 (2021) 104484, https://doi.org/10.1016/j.jmbbm.2021.104484. Elsevier Ltd. (February 2020).

[31] S. Leuridan, et al., Vibration-based fixation assessment of tibial knee implants: a combined in vitro and in silico feasibility study, Med. Eng. Phys. 49 (2017) 109–120, https://doi.org/10.1016/j.medengphy.2017.08.007. Elsevier Ltd.
[32] G. Liu, M. Xiang, H. Li, A Study on Sliding Wear of Ultrahigh Molecular Weight Polyethylene / Polypropylene Blends 44(1), 2004, pp. 197–208.
[33] S. Bao Lu, et al., An 11-year minimum follow-up of the Charite III lumbar disc replacement for the treatment of symptomatic degenerative disc disease, Eur. Spine J. 24 (9) (2015) 2056–2064, https://doi.org/10.1007/s00586-015-3939-5.
[34] G.M. Malham, R.M. Parker, Early experience with lateral lumbar total disc replacement: utility, complications and revision strategies, J. Clin. Neurosci. 39 (2017) 176–183, https://doi.org/10.1016/j.jocn.2017.01.033. Elsevier Ltd. (September 2011).
[35] M. Mbogori, et al., Poly-ether-ether-ketone (PEEK) in orthopaedic practice- a current concept review, J. Orthopaedic Rep. 1 (1) (2022) 3–7, https://doi.org/10.1016/j.jorep.2022.03.013. Elsevier.
[36] P. Moghadas, et al., Friction in metal-on-metal total disc arthroplasty: effect of ball radius, J. Biomech. 45 (3) (2012) 504–509, https://doi.org/10.1016/j.jbiomech.2011.11.045. Elsevier.
[37] P.M. Moghadas, et al., Polymer-on-metal or metal-on-polymer total disc arthroplasty: does it make a difference? Spine 37 (21) (2012) 1834–1838, https://doi.org/10.1097/BRS.0b013e318257fdd3.
[38] S. Momon, et al., Unsupervised and supervised classification of AE data collected during fatigue test on CMC at high temperature, Compos. A: Appl. Sci. Manuf. 43 (2) (2012) 254–260, https://doi.org/10.1016/j.compositesa.2011.10.016. Elsevier Ltd.
[39] I. Nakahara, et al., In vivo implant fixation of carbon fiber-reinforced PEEK hip prostheses in an ovine model, J. Orthop. Res. 31 (3) (2013) 485–492, https://doi.org/10.1002/jor.22251.
[40] K.S. Narendra, K. Parthasarathy, Learning automata approach to hierarchical multiobjective analysis, IEEE Trans. Syst. Man Cybernet. (1991) 263–272, https://doi.org/10.1109/21.101158.
[41] K.A. Olorunlambe, D.E.T. Shepherd, K.D. Dearn, A review of acoustic emission as a biotribological diagnostic tool, Tribol. Mater. Surf. Interface 13 (3) (2019) 161–171, https://doi.org/10.1080/17515831.2019.1622914. Taylor & Francis.
[42] H.T. Ouyang, Nonlinear autoregressive neural networks with external inputs for forecasting of typhoon inundation level, Environ. Monit. Assess. 189 (8) (2017), https://doi.org/10.1007/s10661-017-6100-6.
[43] G. Patzer, M. Woydt, New methodologies indicating adhesive wear in load step tests on the translatory oscillation tribometer, Lubricants 9 (10) (2021), https://doi.org/10.3390/lubricants9100101. Available at.
[44] M. Petrica, et al., Studies on tribological behavior of PEEK and PE-UHMW, AIP Conf. Proc. 1779 (2016), https://doi.org/10.1063/1.4965533 (October 2016).
[45] J. Reeks, H. Liang, Materials and their failure mechanisms in total disc replacement, Lubricants 3 (2) (2015) 346–364, https://doi.org/10.3390/lubricants3020346.
[46] G.W. Rodgers, et al., Acoustic emission monitoring of total hip arthroplasty implants, in: IFAC Proceedings Volumes, IFAC, 2014, pp. 4796–4800, https://doi.org/10.3182/20140824-6-ZA-1003.00928.
[47] C. Rowland, et al., Dynamic health monitoring of metal on metal hip prostheses using acoustic emission, in: 26th European Conference on Acoustic Emission Testing, 2004, pp. 465–467.
[48] H.J. Schwalbe, G. Bamfaste, R.P. Franke, Non-destructive and non-invasive observation of friction and wear of human joints and of fracture initiation by acoustic emission, Proc. Inst. Mech. Eng. H J. Eng. Med. 213 (1) (1999) 41–48, https://doi.org/10.1243/0954411991534799.
[49] L.-K. Shark, H. Chen, J. Goodacre, Discovering differences in acoustic emission between healthy and osteoarthritic knees using a four-phase model of sit-stand-sit movements, Open Med Inform J 4 (2010) 116–125, https://doi.org/10.2174/1874431101004010116.
[50] L.K. Shark, H. Chen, J. Goodacre, Knee acoustic emission: a potential biomarker for quantitative assessment of joint ageing and degeneration, Med. Eng. Phys. 33 (5) (2011) 534–545, https://doi.org/10.1016/j.medengphy.2010.12.009. Institute of Physics and Engineering in Medicine.
[51] S.R. Simon, et al., "Stiction-friction" of total hip prostheses and its relationship to loosening, J. Bone Joint Surg. 57 (2) (1975) 226–230, 57-A(2).
[52] R. Siskey, et al., Are PEEK-on-ceramic bearings an option for total disc arthroplasty? An in vitro tribology study, Clin. Orthop. Relat. Res. 474 (11) (2016) 2428–2440, https://doi.org/10.1007/s11999-016-5041-7. Springer US.
[53] R. Unnporsson, Hit detection and determination in AE bursts, in: W. Sikorski (Ed.), Acoustic Emission, IntechOpen, Rjeka, 2013, https://doi.org/10.5772/54754.
[54] H. Xin, D.E.T. Shepherd, K.D. Dearn, PEEK (polyether-ether-ketone) based cervical total disc arthroplasty: contact stress and lubrication analysis, Open Biomed. Eng. J. 6 (2012) 73–79, https://doi.org/10.2174/1874230001206010073.